Cellulose nanocrystals from native and mercerized cotton

Somia Haouache, Clara Jimenez-Saelices, Fabrice Cousin, Xavier Falourd, Bruno Pontoire, Karine Cahier, François Jérome, Isabelle Capron

Cellulose nanocrystals from native and mercerized cotton

Somia Haouache[1,2], Clara Jimenez-Saelices[1], Fabrice Cousin[3], Xavier Falourd[1], Bruno Pontoire[1], Karine Cahier[1], François Jérome[2] and Isabelle Capron[1*]

[1]*UR1268 Biopolymères Interactions Assemblages, INRAE, 44316 Nantes, France*

[2]*Institut de Chimie des Milieux et Matériaux de Poitiers, Université de Poitiers, 86073 Poitiers, France*

[3]*Laboratoire Léon Brillouin, Université Paris-Saclay, CEA-Saclay, Gif-sur-Yvette, France*

*****Correspondence: isabelle.capron@inrae.fr; Tel.: +33-24067-5095; orcid: 0000-0001-9145-3803

Abstract: Nanocelluloses occur under various crystalline forms that are currently being selectively used for a wide variety of high performance materials. In the present study, two cellulose fibers (CF-I) were mercerized by alkaline treatment (CF-II) without molar mass variation (560,000 g/mol) and both were acid hydrolyzed, forming cellulose nanocrystals in native (CNC-I) and mercerized (CNC-II) forms. This study focuses on the detailed characterization of these two nanoparticle morphologies (light and neutron scattering, TEM, AFM), surface chemistry (zetametry and surface charge), crystallinity (XRD, ^{13}C NMR), and average molar mass coupled to chromatographic techniques (SEC-MALLS-RI, A4F-MALLS-RI), revealing variations in the packing of the crystalline domains. The crystal size of CNC-II is reduced by half compared to CNC-I, with molar masses of individual chains of 41,000 g/mol and 22,000 g/mol for CNC-I and CNC-II, respectively, whereas the same charged surface chemistry is measured. This study gives an example of complementary characterization techniques as well as results to help decipher the mechanism involved in mercerization.

Keywords: *cellulose nanocrystals, mercerization, cellulose II, biobased nanoparticles, nanostructuration.*

1. Introduction

Cellulose is a linear homopolysaccharide of D-glucopyranose units connected by β(1-4) glycosidic bonds (Habibi, Lucia, and Rojas 2010; Moon et al. 2011; Nishiyama 2009). It is stabilized by an inter- and intramolecular complex network of hydrogen bonds and van der Waals interactions.

According to the association type, cellulose exists in six crystalline forms called cellulose I, II, III-I, III-II, IV-I and IV-II (Kroon-Batenburg, Bouma, and Kroon 1996). Cellulose I corresponds to fibrillary native cellulose with parallel oriented chains. The other forms are obtained by conversion of type I by chemical and/or thermal treatments (Atalla and VanderHart 1999; Gardner and Blackwell 1974; Nishiyama, Langan, and Chanzy 2002). Cellulose I can undergo an irreversible transition into a more thermodynamically stable crystalline form, cellulose II, by two distinct processes: regeneration or mercerization. Mercerization involves intracrystalline swelling of the cellulose in concentrated aqueous NaOH where the limit concentration depends on the temperature between 8-15%, with lower temperatures that allow transformation at lower concentrations (Duchemin 2015; Warwicker 1967) and where chains change their orientation from original parallel chains

of cellulose I to antiparallel chains ~~(opposite polarity)~~ (Fink and Philipp 1985; Kolpak, Weih, and Blackwell 1978; Stipanovic and Sarko 1976). The mechanism of mercerization has long been studied. An interdigitation mechanism was first proposed by Okano and Sarko (Okano and Sarko 1985) . NaOH is absorbed, converting cellulose I into a swollen structure in which all contacts between adjacent chains are removed. Once NaOH has been removed by washing with water, a bi-oriented cellulose II structure is obtained (P. Langan, Nishiyama, and Chanzy 1999; Paul Langan, Nishiyama, and Chanzy 2001).

Nishiyama et al. (Nishiyama, Kuga, and Okano 2000) proposed a molecular association in Na-Cellulose where van der Waals' interaction is the driving force of the formation of cellulose II. The effect of mercerization on crystallinity was investigated for different cellulose sources (J. F. Revol, Dietrich, and Goring 1987). All cellulose II obtained had a narrow range of crystallinity and, a constant crystal size. The crystallinity index for the mercerized celluloses remained in a narrow range of 0.50-0.66, whereas it varied from 0.41 to 0.95 for the native cellulose. The crystal size was approximately constant for the mercerized celluloses, from 3.4 nm to 4.4 nm, whereas it varied from 2.9 nm to 15.4 nm in native celluloses. The result is that in the case of highly crystalline cellulose, mercerization reduces crystallinity and crystal size, whereas in the case of low crystallinity cellulose, mercerization increases crystallinity and the size of the crystal. These trends would not be expected if the conversion of cellulose I to cellulose II was simply a change in conformation of the chain or arrangement of atoms. These results are more in line with the idea that mercerization involves a complete destruction of the structure of cellulose I by separation of the molecular chains, followed by the reforming of the crystalline structure in the form of cellulose II. These results are consistent with the hypothesis that mercerization involves a mixture of adjacent and antiparallel cellulose microfibers (Okano and Sarko 1985).

Type II cellulose nanocrystals have already been obtained from acid hydrolysis (Sebe, Ham-Pichavant et al. 2012) or after mercerization of fibers (Neto et al. 2016) . Sèbe et al. (Sèbe et al. 2012) prepared CNC samples using nine different conditions involving H_2SO_4 at concentrations varying from 62 to 66% and up to 120 min. One of them led to CNC-II only (not a mixture of CNC-I and CNC-II). The resulting nanocrystals (CNC-II) were found to be smaller than CNC-I and were ribbon-shaped with rounded tips and larger crystallites, whereas Neto et al. (Neto et al. 2016) described CNC-II as being shorter (from 240 nm to 132 nm) and broader (from 15 nm to 19 nm), with identical thickness (around 4 nm), and with an increased crystallinity from 56% to 68%. For Li et al. (Li et al. 2018), the mercerized CNCs were even much smaller (19 nm in length and 11 nm in width) with ellipsoid shapes.

CNCs are predicted to have a major impact in the coming years, and variability will be a key of this development. Recent reviews show the interest of the selective modification of the reducing end (Heise et al. 2021; Tao et al. 2020) of CNC-I. A growing interest is now focused on CNC-II with the hemiacetal form at the two extremities. A precise control of their various forms is therefore of great importance but the transition mechanism is still a matter of debate. In order to better understand the mechanism involved in mercerization, it is consequently of interest to compare different packs of data produced using both different and similar hydrolyses. But also to compare the results obtained from different technics. For example, the ratio of crystalline regions to total fibrils of cellulose (the crystallinity index) is usually investigated by X-ray diffraction and solid-state 13C-NMR experiments (Park et al. 2010; Zugenmaier 2008). The first one is based on the detection of a diffraction plane, which considers structuration of several glucose residues. The second one is based on the variation of the chemical shift associated with the angles of the glycosidic bond. These two techniques that observe cellulose at two different scales are quite complementary. In the present study, native (CF-I) and mercerized (CF-II) cotton fibers are both hydrolyzed using the same sulfuric acid hydrolysis process, leading to CNC-I and CNC-II. A full set of complementary

techniques is described and used to precisely characterize the morphology, molar mass, structure, surface charge and degree of polymerization of both nanocrystals.

2. Materials and Methods

Materials: The native cotton cellulose fibers were obtained from Buckeye Technology Inc., USA. All reactants had a purity of above 95% and were acquired from Sigma Aldrich and used without further purification. Ultrapure water was produced with the Milli-Q reagent system (18.2 MΩ cm, Millipore Milli-Q purification system).

Cellulose sample preparation: Native cotton cellulose fiber (CF-I) was mercerized (CF-II) according to a protocol similar to that described by Neto et al. (Neto et al. 2016). Ten grams of CF-I were introduced into 300 mL of 20 wt% NaOH and mechanically stirred for 5 h at 25°C. The mixture was washed several times with distilled water in order to remove the NaOH solution, and then dried at 40°C for 48 h. This conversion was carried out with a yield of 100%.

Preparation of cellulose nanocrystals (CNC-I and CNC-II): Both CNCs were prepared by hydrolysis with sulfuric acid according to the method of Revol et al. (J.-F. Revol et al. 1992) with minor modifications. Briefly, cellulose nanocrystals (CNC-I and CNC-II) were prepared under the same conditions from fibers (CF-I and CF-II, respectively) using sulfuric acid hydrolysis at 64% at 68°C under stirring for 20 min. After hydrolysis, the suspensions were washed by centrifugation, dialyzed to neutrality against Milli-Q water for 2 weeks, and deionized using mixed bed resin (TMD-8). The final dispersion was sonicated for 10 min, filtered and stored at 4°C. The yield was 64% and 40% for CNC-I and CNC-II, respectively.

Cellulose sample characterization

X-ray Diffraction. The determination of crystalline type, crystallinity index and crystal size of the different samples was performed by X-ray Diffraction (XRD) analysis using a Bruker D8 Discover diffractometer (Karlsruhe, Germany) equipped with a VANTEC 500 2D detector. X-ray radiation, CuKα1 (λ = 0.15406 nm), produced in a sealed tube at 40 kV and 40 mA, was selected and parallelized using crossed Göbel mirrors and collimated to produce a beam of 300 or 500 µm in diameter. The suspensions of nanocrystals were freeze-dried and then pressed at room temperature to obtain dense pellets, while the fibers were used as such. The diffraction patterns were recorded for 10 min over a range from 3° to 40° (2θ). The recorded intensity was normalized by the total peak area to eliminate the influence of the thickness variation and the absorption coefficient of the samples. The X-ray crystallinity index (CI_{XRD}) was estimated from the crystalline to amorphous areas using Origin (v8.0891) software.

Solid-state NMR CP-MAS. The NMR experiments were carried out on an Avance III-400 MHz spectrometer (Bruker; France) operating at 100.62 MHz for 13C, equipped with a double-resonance H/X CP-MAS 4-mm probe for CP-MAS (Cross-Polarization Magic Angle Spinning) solid-state experiments. The samples were wetted and spun at 12,000 Hz at room temperature.

CP-MAS spectra were acquired with a contact time of 1.5 ms and over an accumulation of 2048 scans separated by a recycling delay of 10 s. The carbonyl carbon was set to 176.03 ppm through external glycine calibration. NMR spectra deconvolution was performed using PeakFit® (v.4.11) software (Systat Software, Inc., USA). Peak chemical shifts were assigned according to (Larsson et al. 1999; Newman and Davidson 2004). The

NMR crystallinity index of CF and CNC was calculated according to (Larsson et al. 1999; Zuckerstätter et al. 2013).

Conductometry. The hydrolysis of the cellulose with sulfuric acid makes it possible to obtain a colloidal suspension of the nanometric-sized crystals with SO3- charges on their surface. The measurement of the quantity of charges on the CNC surface charge was performed by conductometric titration with a 0.001 M NaOH solution using a TIM900 titration manager and a CDM230 conductimeter equipped with a CDC749 conductivity cell.

Zeta Potential (ζ-potential). ζ-potential experiments were performed with a Malvern NanoZS instrument. All measurements were made at a temperature of 20°C with a detection angle of 12.8°. CNC dispersions of 1 g/L at pH = 7 were prepared at 20°C and filtered by 5 µm. Each sample was measured a total of five times. The confidence interval (error) presented is the standard deviation of samples measured in triplicate.

Asymmetrical flow field-flow fractionation coupled to Multi-Angle Laser Light Scattering and Refractive Index (A4F-MALLS-RI) detection. An AF4 instrument was coupled with two online detectors: a MALLS instrument (DAWN Heleos II) fitted with a K5 flow cell and a GaAs laser (λ = 663 nm), and a refractometric detector operating at the same wavelength (Optilab T-rEX) from Wyatt Technology (Santa Barbara, CA, USA). The AF4 instrument consisted of an AF4 channel (275 mm-long), a 350-µm-thick spacer and a regenerated cellulose membrane with a nominal cut-off of 10 kDa (Millipore, Bedford, MA, USA). The refractive index increment dn/dc was 0.146 mL/g, a value classically used for glucans in water **(Paschall and Foster 1952)**. The AF4 channel flow, cross flow, sample injection and focus flow were controlled with a Wyatt Eclipse AF4 flow chassis, a pump and an autosampler from ThermoFisher Scientific (Waltham, MA, USA). CNC dispersions of 0.5 g/L in water were prepared at 20°C and systematically freshly sonicated (amplitude 5, 8 s, 2 on/1 off) before being injected. Each sample was measured a total of two times. The weight and number-average molar masses ($\mathbf{\bar{M}_w}$,$\mathbf{\bar{M}_n}$) and the polydispersity ($\mathbf{\bar{M}_w}/\mathbf{\bar{M}_n}$) of CNCs were determined with Wyatt ASTRA® software (v. 6.1.4) with Zimm extrapolation of order 1.

Size Exclusion Chromatography coupled to Multi-Angle Laser Light Scattering and Refractive Index (SEC-MALLS-RI) detection. The determination of molar mass distribution of chains of cellulose in DMAc/LiCl was carried out at room temperature using an OMNISEC system (Malvern). The size exclusion chromatography (SEC) (OMNISEC Resolve, Malvern) system was coupled with a multi-angle laser light scattering detector (MALLS, Malvern) and OMNISEC Reveal devices (Malvern). The SEC columns used were Viscoteck Tguard, LT4000L, LT5000L and LT7000L. The mobile phase used for SEC was N,N-dimethylacetamide (DMAc) (HPLC grade) containing lithium chloride (LiCl) (0.9% v/w), that had been filtered through 0.6-µm polypropylene prefilters. This eluant was chosen because it solubilizes cellulose without significant depolymerization during the dissolution process or during storage at room temperature for long periods (Dupont and Harrison 2004; Yanagisawa and Isogai 2005). Calculation of weight- and number-average molar masses ($\mathbf{\bar{M}_w}$,$\mathbf{\bar{M}_n}$) and polydispersity ($\mathbf{\bar{M}_w}/\mathbf{\bar{M}_n}$) of samples were performed with a dn/dc value of 0.136 mL/g (Hasani et al. 2013) and determined with OMNISEC software (v.10.30) with Zimm extrapolation of order 2.
Cellulose was solubilized in the DMAc/LiCl (9% v/w) (Dawsey and McCormick 1990; Medronho and Lindman 2015) via solvent exchange steps H2O/Met-OH/DMAc CF-I and CF-II and H2O/Et-OH/DMAc for CNC-I and CNC-II.
For fibers, 100 mg (dry content) of CF-I and CF-II were washed with 30 mL methanol, and the excess of methanol was removed by filtration on fritter n° 3. This step was repeated

three times. The recovered pellet was washed three times with 30 mL of DMAc for solvent exchange, and the excess of DMAc was removed by filtration on fritter n° 3. After solvent exchange steps, 10 mL of D MAc/LiCl (9% v/w) were added to the vial containing the sample and allowed to stir magnetically at 4°C for dissolution.
For CNCs, the samples in the form of aqueous suspensions were freeze-dried. The dry extract obtained (approximately 20 mg) was washed with ethanol, and the excess of ethanol was removed by centrifugation (2220 g for 15 min at 20 °C) **(Hasani et al. 2013)**. This step was repeated twice and the material was then put in DMAc for solvent exchange under magnetic stirring at room temperature overnight. The excess of DMAc was removed by centrifugation (2220 g for 15 min at 20°C). After the solvent exchange steps, 2 mL of DMAc/LiCl 9% (v/w) were added to the vial containing the sample and allowed to stir magnetically at 4°C for dissolution.
The final concentration of the samples was 10 g/L. The dissolution was stopped by the addition of pure DMAc. The final concentration of samples in DMAc/LiCl (0.9% v/w) was 1 g/L. Before injection, the samples were filtered through a 0.45-µm polytetrafluoroethylene (PTFE) membrane filter.

Transmission Electron Microscopy (TEM). Droplets of CNC suspensions at 0.8 g/L were deposited on freshly glow-discharged carbon-coated microscope grids (200 mesh, Dalta Microscopies, France) for 2 min. The excess liquid was removed by filter paper, negatively stained with an aqueous solution of phosphotungstic acid at 10 g/L for 2 min and dried just before TEM observation. We used a JEOL type transmission electron microscope (JEM-1230) operating at a voltage of 80 keV. The average dimensions (length and width) of the CNCs were determined from TEM image analysis of approximately 350 particles using ImageJ software.

Atomic Force Microscopy (AFM). To determine the average thicknesses of the nanocrystals, the suspensions were diluted to 0.05 g/L and then deposited on mica substrates. The measurements were carried out at room temperature by an Innova AFM (Bruker) using a monolithic silicon tip (TESPA, Bruker, spring constant k = 42 N/m, frequency f0 = 320 kHz). Image processing was performed with WSxM 5.0 software.

Small Angle Neutron Scattering (SANS) experiments. SANS experiments were carried out at room temperature using the small-angle PA20 and PAXY diffractometers at the Laboratoire Léon Brillouin (CEA/CNRS) in Saclay (France). Three configurations were used for PA20, covering a Q range from 0.0006 and 0.44 Å−1 (6 Å at 1.1 m, 6 Å at 8 m, and 15 Å at 17.5 m), where Q is the wave vector ($Q = 4\pi \sin \theta/2$, where θ is the scattering angle and λ is the neutron wavelength), and four configurations for PAXY, covering a Q range from 0.002 and 0.5 Å−1 (5 Å at 1 m, 5 Å at 3 m, 8.5 Å at 5 m and 15 Å at 6.7 m). CNC dispersions of 2 g/L in 2 mM NaCl were prepared at 20°C and then extensively dialyzed against D2O to obtain the best possible contrast as well as to reduce the incoherent scattering as much as possible, and then systematically freshly sonicated for 10 s and loaded in quartz cells (Hellma) with small path lengths (1 and 2 mm). To determine the CNC dimensions, the data were fitted with Sasview software. Several fitting models were tried using the form factor of a parallelepiped with a rectangular section, averaged over all space orientations, and constituting a perfectly fitting model of the rod-like CNCs (Cherhal, Cousin, and Capron 2015). Aggregation experiments in solution were performed on suspensions at 2 g/L of CNC-I and CNC-II in 2, 50 and 100 mM NaCl. The suspensions were measured after sonication.

3. Results

3.1 Structural description

The XRD patterns of native, mercerized and hydrolyzed cotton samples are shown in Fig. 1.

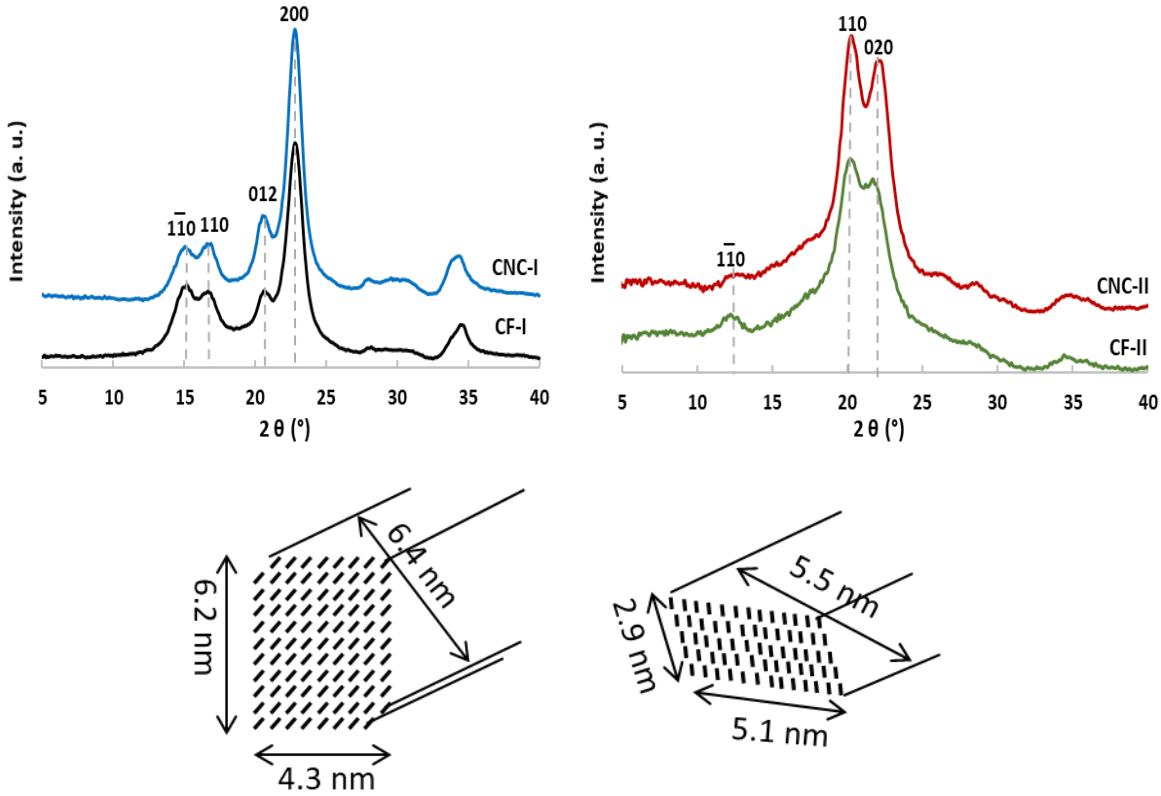

Figure 1. X-ray diffraction patterns of cotton fibers in native (CF-I) and mercerized CF-II forms and their respective hydrolyzed cellulose nanocrystals in the native (CNC-I) and mercerized (CNC-II) forms, and cross-sections of elementary crystallites deduced from the analysis of peak broadening (the indexation of corresponding lattice planes is described in Supporting Information).

The diffraction patterns of CF-I and CNC-I are typical of cellulose I with the presence of diffraction peaks at 15.1°, 16.9°, 20.7° and 22.8°, corresponding to (1-10), (110), (012/102) and (200) crystallographic planes, respectively. After mercerization, the crystallinity index (CI_{XRD}) of CF-II decreased. For the mercerized sample, CF-II and CNC-II at 12.3°, 20.0° and 21.7° corresponded to the (1-10), (110) and (020) reflections, respectively (Duchemin 2015; Isogai et al. 1989; Nishiyama, Kuga, and Okano 2000), whereas traces of cellulose I residuals can be recognized at 15.1° and 16.9° (Fig. 1). This allomorphic modification was achieved without loss in mass (Table 1). XRD peak analysis (see values in SI) allowed representation of the crystals (Fig. 1). The (1-10) and (110) crystalline planes have interplane dimensions of 0.61 nm and 0.54 nm, respectively (Goussé et al. 2002; Sugiyama, Vuong, and Chanzy 1991). Similarly, for CNC-II, the distances for (1-10) and (110) are 0.72 nm and 0.44 nm, respectively (Kolpak, Weih, and Blackwell 1978; P. Langan, Nishiyama, and Chanzy 1999; Sèbe et al. 2012).

After sulfuric acid hydrolysis of the fibers, the XRD results showed an increase of the crystallinity index (CI_{XRD}). For the native form, 64% of the cellulosic material was recovered after hydrolysis, whereas the CI_{XRD} only increase by 5% (from CF-I to CNC-I). The hydrolysis then affects amorphous as well as crystalline domains.
Considering fibers, all the material was recovered after mercerization (yield of 100%). However, after acid hydrolysis, only 40% of the initial material was recovered, while the CI_{XRD} increased by 30% (from CF-II to CNC-II). Mercerization leads to fibers that are more susceptible to acid hydrolysis, probably due to lower organization. Moreover, as can be observed in other studies (French 2014; Neto et al. 2016), mercerization drastically reduces crystallinity as well as the crystal dimensions of the cotton.

Table 1: Weight fraction (yield) recovered after treatment, crystallinity index (CI) calculated from XRD (CIXRD), Mean CI calculated from solid-state NMR (13C CP-MAS) spectra (CINMR). Deconvolution of the C4 region of 13C CP-MAS spectra.

Samples	Yield (%)	CI_{XRD} (%)	CI_{NMR} (%)	Deconvolution of the C4 region		
				crystalline	paracrystalline intermediary domain	amorphous
CF-I	-	60	67	25%	42%	26% Acc + 7% inAcc
CNC-I	64	65	75	36%	39%	25%
CF-II	100	40	72	58%	14%	28%
CNC-II	40	70	85	74%	11%	15%

Figure 2 shows the 13C CP-MAS NMR spectra of CF-I and CF-II and confirms the mercerization process with the two peaks at 88.1 and 86.9 ppm in the CF-II spectrum that are characteristic of type II cellulose (Ibbett, Domvoglou, and Fasching 2007; Newman and Davidson 2004). CF-I had a CI_{NMR} of 67%, and this crystallinity increased after acid hydrolysis. For CF-II, this CI_{NMR} increased up to 72% after mercerization and up to 85% after subsequent hydrolysis (CNC-II preparation).
The signals in the 86-92 ppm region that refer to crystalline domains were further decomposed. This deconvolution analysis discriminates an "in-core" ordered region from a "paracrystalline" organization described as having an intermediate order between amorphous and crystalline cellulose (Zuckerstätter et al. 2013) (Fig. 2). According to this analysis, original CF-I is characterized by a CI_{NMR} of 67% composed of 25% of a pure crystalline domain and 42% of a so-called paracrystalline domain (Table 1). The remaining 33% are divided into 26% of accessible and 7% of inaccessible amorphous domains.
After acid hydrolysis, an increase in the relative area of crystalline peaks at 86-92 ppm is observed, and the CI_{NMR} increased in accordance with XRD results. However, the selective analysis of crystalline and paracrystalline structures shows that the paracrystalline organization is only slightly decreased. The increase in crystallinity between CF-I and CNC-I is then correlated with a loss of the amorphous part, since the paracrystalline domains are much less affected. According to the model proposed by Larsson and also used by Wickholm, paracrystalline domains are structures surrounding nanocrystals in the nanofibers and are less accessible than amorphous domains. After

hydrolysis, the amorphous domain, visible in the 80-86 ppm region, shows only one remaining peak.

After mercerization, a typical spectrum of cellulose II revealed the allomorphic transition. However, the 13C NMR spectrum of CF-II shows a signal characteristic of crystalline C6 of cellulose I representing about 4% of the total C6 signal. This residual crystalline cellulose I-type conformation results from an ineffective penetration of NaOH in crystalline domains; they are potentially dispersed in a random way, as proposed by Kim et al. (Kim et al. 2006).

The mercerization process of the nanofibers results in a slight increase of CI_{NMR} from CF-I to CF-II (Table 1), which is contradictory with XRD results. Simultaneously, a slight decrease of the amorphous contribution from 33% to 28% is observed, and only one peak is observed that refers to only one amorphous type domain. Compared to this, the so-called paracrystalline region, which usually refers to structures surrounding cellulose I nanocrystals, undergoes a sharp decrease from 42% to 14%. The origin and structure of such a state is still not clear (Bregado et al. 2019; Larsson et al. 1999), except that it is intermediate (in terms of mechanical properties, hydrogen bonding and chain ordering) between crystalline and amorphous cellulose. After mercerization, a peak is clearly visible at 85.5 ppm (Fig. 2), referring to that imperfect crystalline region (or, similarly, to an ordered amorphous region). Such a peak was previously observed and attributed to partially ordered cellulose (Ibbett, Domvoglou, and Fasching 2007). The result is that only one type of the amorphous structure remains in a slightly reduced amount, whereas a large part of the paracrystalline-I structure that presumably surrounds the crystalline domains formed by mercerization is lost.

Acid hydrolysis of the mercerized cellulose occurs with a loss of mass (yield: 40%) but without much change in the peak attributed to the intermediate structure. The same trend is then observed for both CNC-I and CNC-II. This was already reported by (Wickholm et al. 2001). It implies that acid hydrolysis removes amorphous regions, contrary to the mercerization process that strongly impacts paracrystalline/intermediate domains. The same fraction of 4% of cellulose I observed in CF-II was recovered in the CNC-II sample.

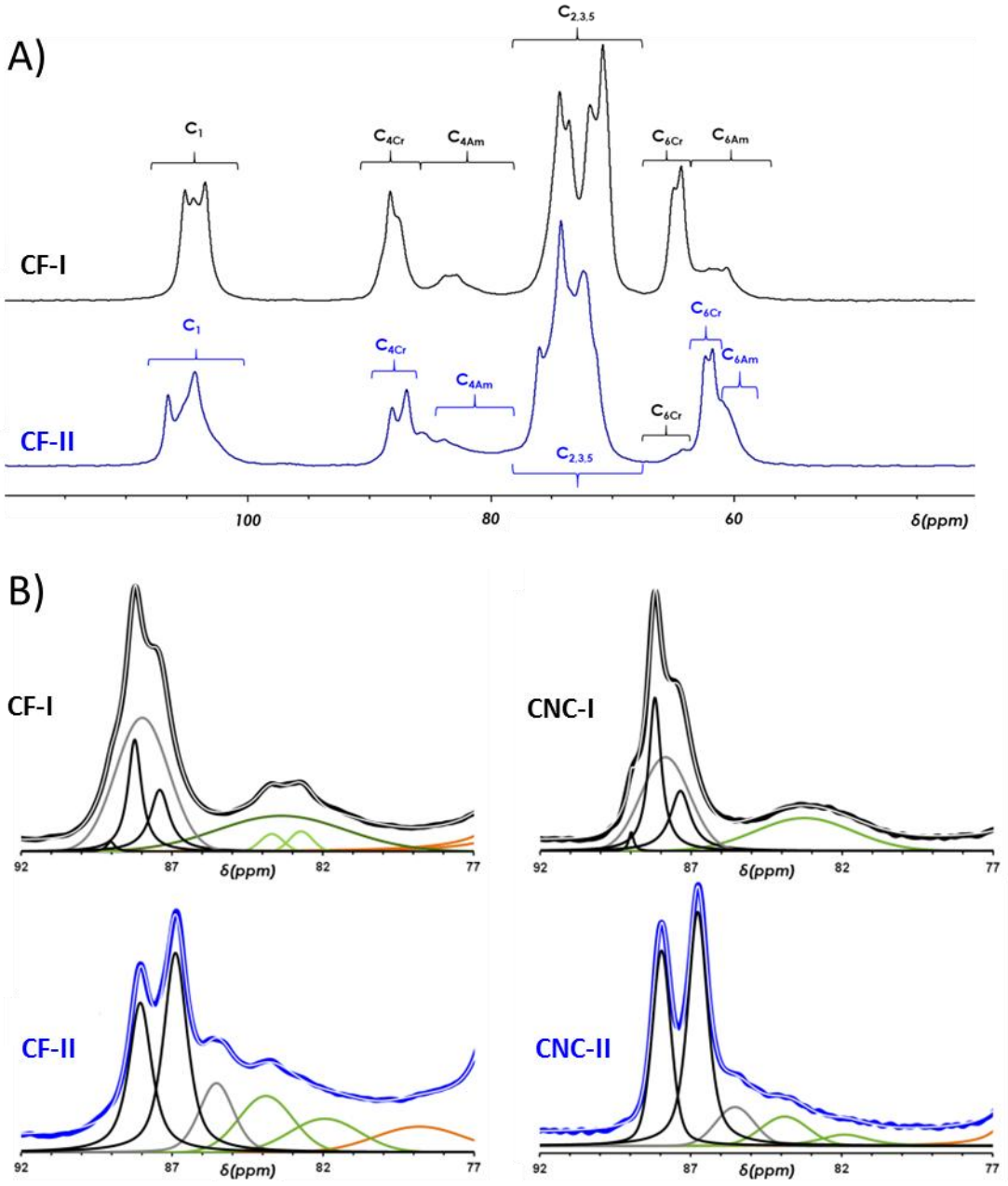

Figure 2. (A) ^{13}C CP-MAS NMR spectra of CF-I and CF-II, and (B) deconvolution of the C4 region of CF-I, CF-II, CNC-I and CNC-II NMR spectra with crystalline forms (black), paracrystalline (gray) and amorphous (green).

However, the results obtained by XRD and NMR are controversial. The loss of crystallinity observed by XRD after mercerization is not observed by NMR (Table 1). In solid-state NMR, ~~considering only the C4 region,~~ chemical shifts are influenced by the conformation of carbon atoms in glycosidic ~~chains~~ bonds, which may be involved in a crystalline, paracrystalline or amorphous structure. For XRD analysis, beyond crystallite orientation, it is the crystal lattice that is directly identified. It is therefore easy to imagine that parts of chains may have conformations related to those of crystal lattices without having a dimension that allows XRD to identify them as such, explaining a higher value of CI by NMR. The variations observed can then be linked to the ability of each technique to detect imperfect organizations. NMR assumes that all the carbons involved are in crystalline structure which considers very short-scale. It analyzes crystalline and

paracrystalline organizations in the so-called CI_{NMR}, and distinguishes these forms from the amorphous domain with signals shifted to lower ppm values. In contrast, XRD analysis requires longer scale organization since the presence of paracrystalline organizations is included in the widening peaks attributed to amorphous domains.

As a result, a major modification during mercerization comes from this intermediate state that is reformed in smaller amounts after swelling in NaOH and the recrystallization process. In addition, mercerization leads to more crystalline domains that seem to be more discontinuous than the former. Such structures are not fully detected by XRD analysis but assumed by NMR to be globally crystalline. Furthermore, only one amorphous peak is visible after mercerization by NMR, implying only one type of amorphous area. This might reveal a more homogeneous but less organized system, with more imperfections, which is also in accordance with the increased susceptibility to acid hydrolysis of CF-II. After hydrolysis, imperfections are removed and highly crystalline particles are recovered, as detected by both XRD and NMR analyses.

3.2 Molar mass characterization

In order to follow the process at a molecular level, the native and mercerized fibers were dissolved in DMAc/LiCl and injected into a SEC-MALLS-DRI device. This experiment made it possible to determine the molar mass (Mw) distribution of individual cellulosic chains. It may also determine whether the process that involved NaOH at a high concentration had an impact on the glucosidic chain length. The size exclusion fractionation mode implies that larger molecules are the first to elute. Both fibers were found to have an average molar mass of 560,000 g/mol with a low polydispersity (Table 2). Even just a slight shift to higher retention volumes seems to indicate more flexibility of CF-I. However, it is demonstrated here that mercerization treatment of native cellulose fibers through NaOH swelling does not induce any molecular disruption.

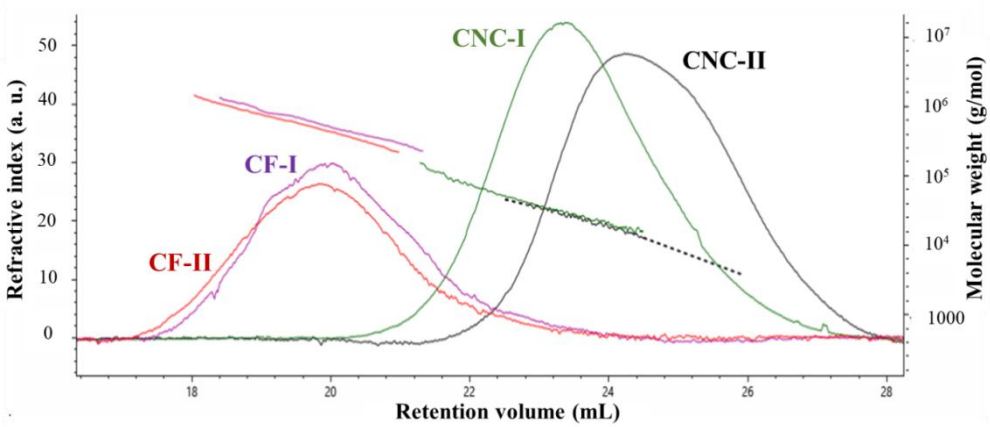

Figure 3. Dissolution profiles of samples obtained by SEC-MALLS-DRI. The two nanofibers (CF-I in purple and CF-II in red) are eluted at low retention volumes, whereas the nanocrystals are eluted at higher elution volumes (CNC-I in green and CNC-II in black).

Table 2. Weight-average molar masses ($\bar{M}_w$), polydispersity ($\bar{M}_w/\bar{M}_n$) and degree of polymerization (DP) of individual chains of cellulosic fibers (CF-I and CF-II) and cellulose nanocrystals (CNC-I and CNC-II) solubilized in DMAc/0.9% LiCl.

Samples	M_w (g/mol)	M_w/M_n	DP_w	DP_n

CF-I	565,000 ± 47,000	1.3	3487	2683
CF-II	556,000 ± 43,000	1.3	3432	2640
CNC-I	41,000 ± 1,000	1.2	253	210
CNC-II	22,000 ± 1,000	1.2	135	112

Similarly, both CNCs were solubilized in DMAc/9% LiCl (v/w) for Mw distribution determination. They logically appear to have a larger retention volume compared to the fibers (Fig. 3), indicating a significant decrease in the hydrodynamic volume of the chains. The acid hydrolysis of the fibers led to a clear decrease of the Mw, from 560,000 g/mol for both fibers, down to 41,000 g/mol for CNC-I and to 22,000 g/mol for CNC-II (Table 2). Contrary to mercerization that did not affect the chain length, the degree of polymerization (DP) of CNC-II is about half as low as CNC-I after the hydrolysis. Furthermore, the Mw distribution curves of CNC-II were shifted to lower retention volumes but superimposed on a large domain, illustrating the same proportion in occupied volume. In other words, CNC-II is similar in conformation but smaller.

Simultaneously, Mw distributions of the CNCs directly in suspension in water (without a solubilization step) were obtained using A4F-MALLS-DRI analysis (Fig. 4). Since the fractionation is carried out by a cross-flow device, the smaller molecules were the first to elute. The shift to a lower elution time for CNC-II compared to CNC-I confirmed the lower hydrodynamic volumes of CNC-II. The Mw measured were also much lower (Table 3), with 36.106 g/mol and 11.106 g/mol for CNC-I and CNC-II, respectively. These values are in agreement with the results found by the SEC-MALLS-DRI device.

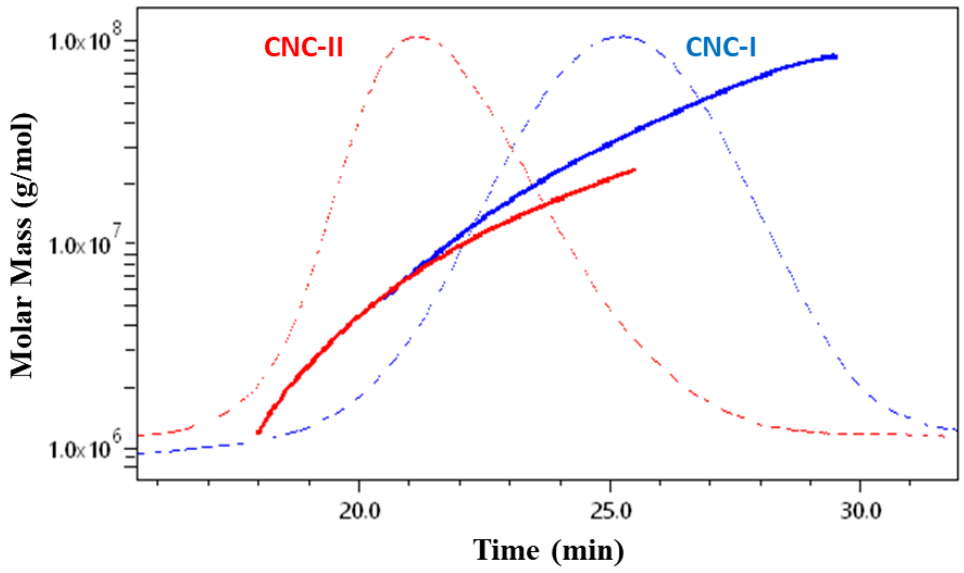

Figure 4. Distribution of molar masses of suspensions of CNC-I (blue) and CNC-II (red) in water, and RI signal (dotted curves).

When dividing the molar mass obtained in crystalline form from both CNCs (Table 3) to that of their individual chains (Table 2), the packing appeared to decrease from 878 to 500 chains for CNC-I and CNC-II, respectively. This is a very high value compared to the dimensions of the elementary CNCs, revealing that some aggregation still remains.

However, it clearly appears that the mercerized CNCs are two to three times smaller in length and packing. The result is that the crystalline domains in NF-II are shorter, with a DP of less than half of those in NF-I.

3.3 Characterization of cellulose nanocrystal morphology

The morphology of native and mercerized CNCs was characterized and compared by TEM, AFM and SANS. Figure 5 shows TEM and AFM images of native and mercerized CNCs. Both CNCs are in the form of rigid rods with shorter CNC-II. The average lengths of 118 ± 65 nm and 65 ± 22 nm were determined for CNC-I and CNC-II, respectively (Table 3). This is in accordance with previous results (Neto et al. 2016). When selecting individual CNCs, in order to measure elemental nanocrystals, it was found that CNC-I and CNC-II have the same individual width of 7 ± 3 nm. More surprisingly and differently from what was previously reported by (Neto et al. 2016), the average thicknesses found by AFM were 6.0 ± 2.4 nm and 3.4 ± 1.5 nm for CNC-I and CNC-II, respectively (Table 3). The thickness reduced by half of its value is clearly observable.

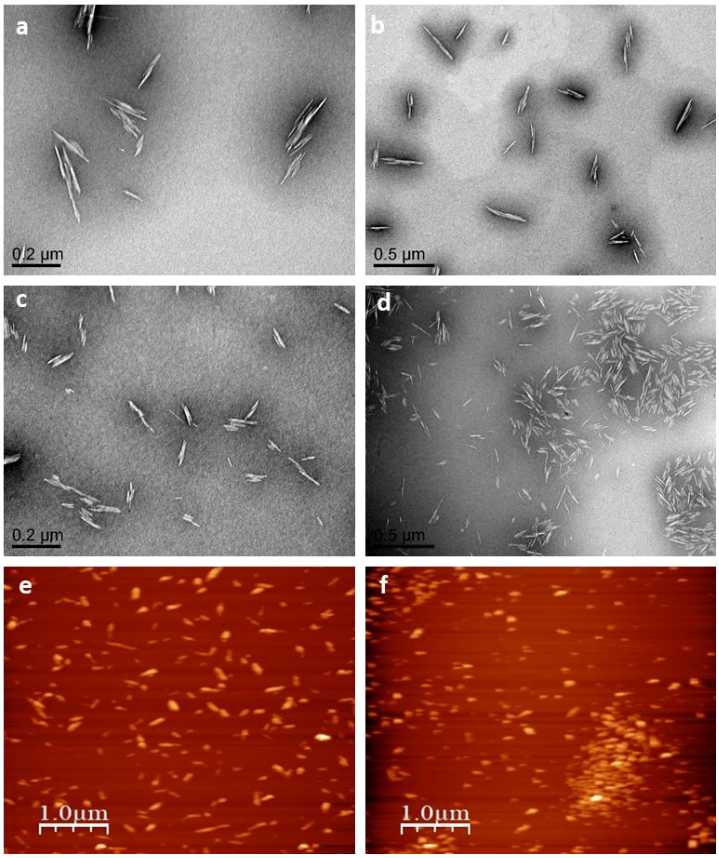

Figure 5. TEM images of CNC-I (a,b) and CNC-II (c,d) and AFM images of CNC-I (e) and CNC-II (f).

Table 3. Weight-average molar masses (Mw) and polydispersity (Mw/Mn) of CNC-I and CNC-II dispersed in water determined by A4F-MALLS-DRI; average dimensions determined from the SANS curve, TEM images and AFM images.

Samples	$\bar{M}_w$	$\bar{M}_w/\bar{M}_n$	Length (nm)	Width (nm)	Thickness (nm)

	(10^6g/mol)		SANS	TEM	SANS	TEM	SANS	AFM
CNC-I	36 ± 1	1.5	175 ± 25	118 ± 65	21 ± 1	7 ±3	6.5 ± 0.5	6.0 ± 2.5
CNC-II	11 ± 1	1.5	75 ± 25	65 ± 22	22 ± 2	7 ±3	3.5 ± 0.5	3.4 ±1.5

The validation of these results was carried out in suspensions of CNCs in water at 2 mM NaCl by the fit of the curves obtained by small angle neutron scattering (SANS) using the parallelepiped form factor (Figure 6). This measurement allows analysis in dilute suspensions without a drying step. CNC-I shows a higher intensity at low q, revealing a higher Mw, and crosses the profile of CNC-II at intermediate Q. For both samples, the best fit obtained confirmed length and thickness values obtained by microscopy. Even if some individual CNCs must be present in suspension, a best fit is obtained for an average width of 21 nm for both samples, corresponding to an average of three to four elementary laterally associated crystals, as already measured (Cherhal, Cathala, and Capron 2015; Elazzouzi-Hafraoui et al. 2007) .The lateral association is then not modified during the mercerization process. The elementary cotton–based CNC-I is generally viewed with a squared cross-section. CNC-II then appears with a rectangular cross-section. The values are in agreement with the results found by A4F-MALLS-DRI and SEC-MALLS-DRI devices.

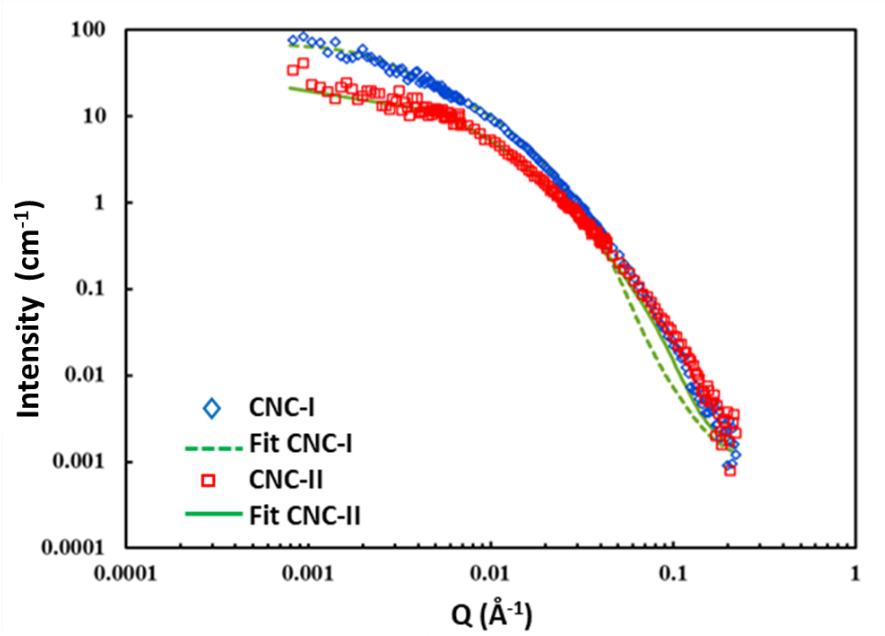

Figure 6. I = f(Q) SANS curves of suspensions of CNC-I and CNC-II in water at 2 g/L in 2 mM NaCl.

3.4. CNC surface charge density

Hydrolysis with sulfuric acid is known to graft anionic sulfate half esters (OSO3−) on to the surface of the CNCs. The same surface charge density is obtained for both CNCs as indicated by the sulfate content of 0.27% and the zeta-potential values of –42 mV for

both CNC-I and CNC-II (Table 4). This implies the same susceptibility of both fiber surfaces to acid treatment.

Table 4. Sulfur content (S), surface charge density (SC) and zeta potential of CNC-I and CNC-II.

Samples	S (%)	SC (mmol/g)	ζ-potential (mV)
CNC-I	0.278 ± 0.09	0.087 ± 0.03	- 42.3 ± 2.7
CNC-II	0.271 ± 0.03	0.085 ± 0.01	- 41.9 ± 1.9

4. Discussion

Table 5: Comparison with other studies in length (L), width (W), thickness (T) and crystallinity index (CI).

	Sèbe et al. (2012)				Neto et al. (2016)				Haouache et al. (present work)			
	L	W	T	CI	L	W	T	CI XRD/NMR	L	W	T	CI XRD/NMR
CNC-I	246	-	5.9	-	240	15	3.8	56/50	175/118	21	6	65/75
CNC-II	153	6.3	4.2	-I	132	19	5.2	68/63	75/65	22	3.5	70/85

Comparing these results with previous ones (Table 5), Sèbe et al. (Sèbe et al. 2012) prepared CNC samples using nine different sulfuric acid conditions. This resulted in a new type of preparation of cellulose II that led to shorter CNCs with rounded tips and larger crystallites but a lower degree of order. This morphology is very different from our mercerized samples. Since we used the same process as Neto et al. (Neto et al. 2016), the results are more similar. These two studies reveal that the nanocrystals are shorter and preserve lateral associations after mercerization, known as an average of trimer associations. However, the thickness was half as much after mercerization, whereas we confirmed by several technics a decrease by half in our experiment.

On the basis of our results, we can determine the average amount of chains per elementary crystal in several ways.

Using the number-average molar mass (Mn) given by A4F-MALLS-RI, and dividing these values by 3, we obtain an average molar mass of $8 \cdot 10^6$ g/mol for the elementary CNC-I, and $2.4 \cdot 10^6$ g/mol for the elementary CNC-II (Table 6). These results, together with those obtained by SEC/MALLS, make it possible to determine the number of cellulosic chains in an elementary crystal: 235 chains per elementary CNC-I and 133 chains per elementary CNC-II. This is large compared to theoretical calculations based on crystal dimensions.

Another calculation considers the CNC section obtained from microscopy and the interchain dimensions. The average CNC thickness is 6.5 nm and 3.5 nm for CNC-I and CNC-II, respectively. The (1-10) and (110) interplane dimensions in CNC-I are 0.61 nm and 0.54 nm, respectively (Goussé et al. 2002; Sugiyama, Vuong, and Chanzy 1991). Similarly, interplane dimensions for CNC-II are 0.72 nm and 0.44 nm for (1-10) and (110), respectively (Kolpak, Weih, and Blackwell 1978; P. Langan, Nishiyama, and Chanzy 1999; Sèbe et al. 2012). Considering that CNC is completely crystalline, this leads to

7x6.5/0.61x0.54=162 cellulose chains per elementary CNC-I and 7x3.5/0.72x0.44=77 cellulose chains for CNC-II.

Calculating average crystalline dimensions from XRD analysis (see Fig. 1), we obtain 4.3x6.2/0.61x0.54=80 cellulose chains per elementary CNC-I and 2.9x5.5/0.72x0.44=50 cellulose chains for CNC-II.

Considering these different results, the microscopy should overestimate the crystal dimension; overestimating also the number of chains per elementary crystals. On the other hand XRD results taking into account the effective crystalline part may not take into account defaults and surface effects underestimating the number of chains per elementary crystals. The effective value should then be somewhere in between that we can estimate at 120 chains/elementary crystals for CNC-I, and 60 chains/elementary crystals for CNC-II.

We couldn't find values to compare such results with other works, regardless of the calculation method, about half of the former number of chains per elementary nanocrystal is recovered after mercerization. The chains are presumably mixed in the global fiber by interdigitation and during crystallization rearrangement on shorter distances with smaller crystals packing less chain. However, they seem more homogeneously distributed along the fiber.

This may indicate that all the chains of the fibril are redistributed during mercerization, forming a globally more regular fiber, but composed of smaller, more discontinuous and bi-oriented crystallites.

Table 6. Number-average molar mass ($\overline{M}_n$) of CNCs, elementary nanocrystals and individual chains, and the number of chains per individual CNC.

CNCs	$\overline{M}_n$ of CNCs (g/mol)	$\overline{M}_n$ of elementary nanocrystals (g/mol)	$\overline{M}_n$ of individual chains (g/mol)	Number of chains/elementary crystals (from Mn)	Number of chains/elementary crystals (from microscopy)	Number of chains/ elementary crystals (from XRD)
CNC-I	$24 \pm 1 \cdot 10^6$	$8 \cdot 10^6$	34,000 ± 1,000	235	162	82
CNC-II	$7 \pm 1 \cdot 10^6$	$2.4 \cdot 10^6$	18,000 ± 1,000	133	77	50

5. Conclusions

Using identical acid hydrolysis on native and mercerized NFs, a panel of techniques is used to show that the mercerization treatment does not degrade cellulosic chains (Mw of 560,000 g/mol) but instead limits the resistance to acid (yield of 64% and 40% for CNC-I and CNC-II, respectively) and impacts the resulting CNCs. The thickness and length of nanocrystals are reduced, preserving the lateral average association corresponding to a trimer (three elementary nanocrystals), and resulting in molar masses of 40,000 g/mol and 11,000 g/mol for CNC-I and CNC-II, respectively. By probing the internal structure, we were able to show more intermediary structures between

ordered and amorphous domains. In addition, the two distinct (accessible/inaccessible) amorphous domains that are detected in cellulose I are not detected in mercerized form, even before acid hydrolysis. This occurs with unchanged surface charge density but a reduction of the crystal thickness by half. Finally, mercerization has a major impact on crystal organization with a much lower chain packing per nanocrystal. Compared to previous works, this article includes additional values notably on molar masses and proposed various comparative techniques. We hope this analysis can further help researchers to characterize their own samples.

Acknowledgements

The authors are grateful to Nadege Beury for AFM images and Emilie Perrin for TEM images with instruments from the BIBS platform (INRAE, Nantes, France), and to Laboratoire Léon Brillouin for providing neutron radiation facilities (CEA-Saclay, Gif sur Yvette, France). They are also grateful to Benoit Duchemin and Yoshiharu Nishiyama for their very stimulating discussions.

Funding

This project received funding from the French National Research Agency (ANR) (CELLOPLASM project, N° ANR-16-CE07-0003-03), including the PhD grant of SH. The authors are also grateful to INRAE for financial support.

Conflicts of interest: No conflicts of interest
Ethics approval: No ethical approval required

References

Atalla, R. H., and David L. VanderHart. 1999. "The Role of Solid State 13C NMR Spectroscopy in Studies of the Nature of Native Celluloses." *Solid State Nuclear Magnetic Resonance* 15(1): 1–19.

Bregado, Jurgen Lange et al. 2019. "Amorphous Paracrystalline Structures from Native Crystalline Cellulose: A Molecular Dynamics Protocol." *Fluid Phase Equilibria* 491: 56–76.

Cherhal, Fanch, Bernard Cathala, and Isabelle Capron. 2015. "Surface Charge Density Variation to Promote Structural Orientation of Cellulose Nanocrystals." *Nordic Pulp & Paper Research Journal* 30(1): 126–31.

Cherhal, Fanch, Fabrice Cousin, and Isabelle Capron. 2015. "Influence of Charge Density and Ionic Strength on the Aggregation Process of Cellulose Nanocrystals in Aqueous Suspension, as Revealed by Small-Angle Neutron Scattering." *Langmuir* 31(20): 5596–5602.

Dawsey, T. R., and Charles L. McCormick. 1990. "The Lithium Chloride/Dimethylacetamide Solvent for Cellulose: A Literature Review." *Journal of Macromolecular Science—Reviews in Macromolecular Chemistry and Physics* 30(3–4): 405–440.

Duchemin, B. J. C. 2015. "Mercerisation of Cellulose in Aqueous NaOH at Low Concentrations." *Green Chemistry* 17(7): 3941–3947.

588 Dupont, Anne-Laurence, and Gabrielle Harrison. 2004. “Conformation and Dn/Dc Determination
589 of Cellulose in N, N-Dimethylacetamide Containing Lithium Chloride.” *Carbohydrate*
590 *polymers* 58(3): 233–243.

591 Elazzouzi-Hafraoui, Samira et al. 2007. “The Shape and Size Distribution of Crystalline
592 Nanoparticles Prepared by Acid Hydrolysis of Native Cellulose.” *Biomacromolecules* 9(1):
593 57–65.

594 Fink, Hans-Peter, and Burkart Philipp. 1985. “Models of Cellulose Physical Structure from the
595 Viewpoint of the Cellulose I→ II Transition.” *Journal of applied polymer science* 30(9):
596 3779–3790.

597 French, Alfred D. 2014. “Idealized Powder Diffraction Patterns for Cellulose Polymorphs.”
598 *Cellulose* 21(2): 885–896.

599 Gardner, K. H., and J. Blackwell. 1974. “The Structure of Native Cellulose.” *Biopolymers: Original*
600 *Research on Biomolecules* 13(10): 1975–2001.

601 Goussé, Cécile et al. 2002. “Stable Suspensions of Partially Silylated Cellulose Whiskers Dispersed
602 in Organic Solvents.” *Polymer* 43(9): 2645–2651.

603 Habibi, Youssef, Lucian A. Lucia, and Orlando J. Rojas. 2010. “Cellulose Nanocrystals: Chemistry,
604 Self-Assembly, and Applications.” *Chemical reviews* 110(6): 3479–3500.

605 Hasani, Merima et al. 2013. “Nano-Cellulosic Materials: The Impact of Water on Their Dissolution
606 in DMAc/LiCl.” *Carbohydrate polymers* 98(2): 1565–1572.

607 Heise, Katja et al. 2021. “Chemical Modification of Reducing End-Groups in Cellulose
608 Nanocrystals.” *Angewandte Chemie International Edition* 60(1): 66–87.

609 Ibbett, Roger N., Dimitra Domvoglou, and Mario Fasching. 2007. “Characterisation of the
610 Supramolecular Structure of Chemically and Physically Modified Regenerated Cellulosic
611 Fibres by Means of High-Resolution Carbon-13 Solid-State NMR.” *Polymer* 48(5): 1287–
612 1296.

613 Isogai, Akira et al. 1989. “Solid-State CP/MAS Carbon-13 NMR Study of Cellulose Polymorphs.”
614 *Macromolecules* 22(7): 3168–3172.

615 Kim, Nam-Hun, Tomoya Imai, Masahisa Wada, and Junji Sugiyama. 2006. “Molecular
616 Directionality in Cellulose Polymorphs.” *Biomacromolecules* 7(1): 274–280.

617 Kolpak, Francis J., Mark Weih, and John Blackwell. 1978. “Mercerization of Cellulose: 1.
618 Determination of the Structure of Mercerized Cotton.” *Polymer* 19(2): 123–131.

619 Kroon-Batenburg, L. M. J., B. Bouma, and J. Kroon. 1996. “Stability of Cellulose Structures Studied
620 by MD Simulations. Could Mercerized Cellulose II Be Parallel?” *Macromolecules* 29(17):
621 5695–5699.

622 Langan, P., Y. Nishiyama, and H. Chanzy. 1999. “A Revised Structure and Hydrogen-Bonding
623 System in Cellulose II from a Neutron Fiber Diffraction Analysis.” *Journal of the American*
624 *Chemical Society* 121(43): 9940–9946.

625 Langan, Paul, Yoshiharu Nishiyama, and Henri Chanzy. 2001. “X-Ray Structure of Mercerized
626 Cellulose II at 1 \AA Resolution.” *Biomacromolecules* 2(2): 410–416.

627 Larsson, Per Tomas et al. 1999. “CP/MAS 13C-NMR Spectroscopy Applied to Structure and
628 Interaction Studies on Cellulose I.” *Solid state nuclear magnetic resonance* 15(1): 31–40.

Li, Xia et al. 2018. “Cellulose Nanocrystals (CNCs) with Different Crystalline Allomorph for Oil in Water Pickering Emulsions.” *Carbohydrate polymers* 183: 303–310.

Medronho, Bruno, and Björn Lindman. 2015. “Brief Overview on Cellulose Dissolution/Regeneration Interactions and Mechanisms.” *Advances in Colloid and Interface Science* 222: 502-502–8.

Moon, Robert J. et al. 2011. “Cellulose Nanomaterials Review: Structure, Properties and Nanocomposites.” *Chemical Society Reviews* 40(7): 3941–3994.

Neto, Wilson Pires Flauzino et al. 2016. “Comprehensive Morphological and Structural Investigation of Cellulose I and II Nanocrystals Prepared by Sulphuric Acid Hydrolysis.” *RSC Advances* 6(79): 76017–76027.

Newman, Roger H., and Tony C. Davidson. 2004. “Molecular Conformations at the Cellulose–Water Interface.” *Cellulose* 11(1): 23–32.

Nishiyama, Yoshiharu. 2009. “Structure and Properties of the Cellulose Microfibril.” *Journal of Wood Science* 55(4): 241–49.

Nishiyama, Yoshiharu, Shigenori Kuga, and Takeshi Okano. 2000. “Mechanism of Mercerization Revealed by X-Ray Diffraction.” *Journal of wood science* 46(6): 452–457.

Nishiyama, Yoshiharu, Paul Langan, and Henri Chanzy. 2002. “Crystal Structure and Hydrogen-Bonding System in Cellulose Iβ from Synchrotron X-Ray and Neutron Fiber Diffraction.” *Journal of the American Chemical Society* 124(31): 9074–9082.

Okano, T., and A. Sarko. 1985. “Mercerization of Cellulose. II. Alkali–Cellulose Intermediates and a Possible Mercerization Mechanism.” *Journal of Applied Polymer Science* 30(1): 325–332.

Park, Sunkyu et al. 2010. “Cellulose Crystallinity Index: Measurement Techniques and Their Impact on Interpreting Cellulase Performance.” *Biotechnology for biofuels* 3(1): 1–10.

Paschall, Eugene F., and Joseph F. Foster. 1952. “Further Studies by Light Scattering of Amylose Aggregates. Particle Weights under Various Conditions.” *Journal of Polymer Science* 9(1): 85–92.

Revol, J. F., A. Dietrich, and D. A. I. Goring. 1987. “Effect of Mercerization on the Crystallite Size and Crystallinity Index in Cellulose from Different Sources.” *Canadian journal of chemistry* 65(8): 1724–1725.

Revol, J.-F. et al. 1992. “Helicoidal Self-Ordering of Cellulose Microfibrils in Aqueous Suspension.” *International journal of biological macromolecules* 14(3): 170–172.

Sèbe, Gilles et al. 2012. “Supramolecular Structure Characterization of Cellulose II Nanowhiskers Produced by Acid Hydrolysis of Cellulose I Substrates.” *Biomacromolecules* 13(2): 570–578.

Stipanovic, Arthur J., and Anatole Sarko. 1976. “Packing Analysis of Carbohydrates and Polysaccharides. 6. Molecular and Crystal Structure of Regenerated Cellulose II.” *Macromolecules* 9(5): 851–857.

Sugiyama, Junji, Roger Vuong, and Henri Chanzy. 1991. “Electron Diffraction Study on the Two Crystalline Phases Occurring in Native Cellulose from an Algal Cell Wall.” *Macromolecules* 24(14): 4168–4175.

Tao, Han et al. 2020. “Reducing End Modification on Cellulose Nanocrystals: Strategy, Characterization, Applications and Challenges.” *Nanoscale horizons* 5(4): 607–627.

Warwicker, J. O. 1967. “Effect of Chemical Reagents on the Fine Structure of Cellulose. Part IV. Action of Caustic Soda on the Fine Structure of Cotton and Ramie.” *Journal of Polymer Science Part A-1: Polymer Chemistry* 5(10): 2579–2593.

Wickholm, Kristina et al. 2001. “Quantification of Cellulose Forms in Complex Cellulose Materials: A Chemometric Model.” *Cellulose* 8(2): 139–148.

Yanagisawa, Masahiro, and Akira Isogai. 2005. “SEC- MALS- QELS Study on the Molecular Conformation of Cellulose in LiCl/Amide Solutions.” *Biomacromolecules* 6(3): 1258–1265.

Zuckerstätter, Gerhard, Nicoleta Terinte, Herbert Sixta, and Kurt Christian Schuster. 2013. “Novel Insight into Cellulose Supramolecular Structure through 13C CP-MAS NMR Spectroscopy and Paramagnetic Relaxation Enhancement.” *Carbohydrate Polymers* 93(1): 122-122–28.

Zugenmaier, Peter. 2008. *Crystalline Cellulose and Derivatives: Characterization and Structures*. Springer.

Figure captions:

Figure 1. X-ray diffraction patterns of cotton fibers in native (CF-I) and mercerized CF-II forms and their respective hydrolyzed cellulose nanocrystals in the native (CNC-I) and mercerized (CNC-II) forms, and cross-sections of elementary crystallites deduced from the analysis of peak broadening (the indexation of corresponding lattice planes is described in Supporting Information).

Figure 2. (A) ^{13}C CP-MAS NMR spectra of CF-I and CF-II, and (B) deconvolution of the C4 region of CF-I, CF-II, CNC-I and CNC-II NMR spectra with crystalline forms (black), paracrystalline (gray) and amorphous (green).

Figure 3. Dissolution profiles of samples obtained by SEC-MALLS-DRI. The two nanofibers (CF-I in purple and CF-II in red) are eluted at low retention volumes, whereas the nanocrystals are eluted at higher elution volumes (CNC-I in green and CNC-II in black).

Figure 4. Distribution of molar masses of suspensions of CNC-I (blue) and CNC-II (red) in water, and RI signal (dotted curves).

Figure 5. TEM images of CNC-I (a,b) and CNC-II (c,d) and AFM images of CNC-I (e) and CNC-II (f)

Figure 6. I = f(Q) SANS curves of suspensions of CNC-I and CNC-II in water at 2 g/L in NaCl 2 mM

Table Captions:

Table 1: Weight fraction (yield) recovered after treatment; crystallinity index (CI) calculated from XRD (CIXRD); mean CI calculated from solid-state NMR (13C CP-MAS) spectra (CINMR); and deconvolution of the C4 region of 13C CP-MAS spectra.

Table 2. Weight-average molar masses ($\bar{M}_w$); polydispersity ($\bar{M}_w/\bar{M}_n$); and degree of polymerization (DP) of individual chains of cellulosic fibers (CF-I and CF-II) and cellulose nanocrystals (CNC-I and CNC-II) solubilized in DMAc/0.9% LiCl.

Table 3. Weight-average molar masses (Mw) and polydispersity (Mw/Mn) of CNC-I and CNC-II dispersed in water determined by A4F-MALLS-DRI; and average dimensions determined from the SANS curve, TEM images and AFM images.

Table 4. Sulfur content (S), surface charge density (SC) and zeta potential of CNC-I and CNC-II.

Table 5. Number-average molar mass ($\bar{M}_n$) of CNCs, elementary nanocrystals and individual chains, and the number of chains per individual CNC